

Article

# Effect of Na<sub>2</sub>O and Rb<sub>2</sub>O on Inclusion Removal in C96V Saw Wire Steels Using Low-Basicity LF (Ladle Furnace) Refining Slags

Changyong Chen, Zhouhua Jiang \*, Yang Li, Meng Sun, Kui Chen, Qi Wang and Huabing Li \*

School of Metallurgy, Northeastern University, Shenyang 110819, China; 1610456@stu.neu.edu.cn (C.C.); liy@smm.neu.edu.cn (Y.L.); sunmengneu@stumail.neu.edu.cn (M.S.); chenku1710497@stumail.neu.edu.cn (K.C.); wangqineu@stumail.neu.edu.cn (Q.W.)

\* Correspondence: jiangzh@smm.neu.edu.cn (Z.J.); lihb@smm.neu.edu.cn (H.L.); Tel.: +86-024-8368-6453 (Z.J.); +86-024-8368-9580 (H.L.)

Received: 18 July 2018; Accepted: 23 August 2018; Published: 3 September 2018



**Abstract:** Inclusion removal and modification of C96V saw wire steel using Na<sub>2</sub>O- and Rb<sub>2</sub>O-containing novel low-basicity LF (ladle furnace) Refining Slags have been researched. The results indicated that the addition of Na<sub>2</sub>O deteriorates inclusion removal; by contrast, the addition of Rb<sub>2</sub>O seems to significantly enhance inclusion removal. In detail, Rb<sub>2</sub>O can improve the cleanliness in the as-quenched C96V saw wire steel melts compared to preexisting synthetic LF refining slag compositions: (i) The average inclusion diameter experienced a remarkable decrease after reaction between the liquid steel and the synthetic LF refining slag; (ii) In addition, the number of inclusions also suffered from a dramatic decrease, with the reaction time increasing from 900 to 2700 s (15-to 45 min); (iii) Furthermore, both of the MnO-SiO<sub>2</sub>-Al<sub>2</sub>O<sub>3</sub> and CaO-SiO<sub>2</sub>-Al<sub>2</sub>O<sub>3</sub> inclusion system mainly concentrated in the low melting zone when the composition of Rb<sub>2</sub>O in synthetic refining slag was ≥5.0 wt%. This is mainly because Na<sub>2</sub>O significantly reduces the viscosity of refining slag, while Rb<sub>2</sub>O increases it. Then, there are two remarkable influences causing the increase of viscosity of refining slag with the addition of Rb<sub>2</sub>O: the inclusions can be sufficiently entrained within the slag once absorbed due to the significant increase in the viscosity; and the slag entrapment during refining process weakened dramatically.

**Keywords:** Na<sub>2</sub>O; Rb<sub>2</sub>O; C96V saw wire steels; LF refining slag; inclusions

## 1. Introduction

In order to obtain a high productivity, higher tensile properties and smaller diameters ( $60 \times 10^{-6}$  m (60 μm) to  $80 \times 10^{-6}$  m (80 μm)) than tire cord are very for saw wire [1]. Therefore, much a higher requirement for inclusion control should be put forward to prevent wire breakage caused by large size or hard inclusions which often initiate breakage during cord drawing and standing processes [2–4]. To this end, a lot of technology has been developed by metallurgical workers, such as Si-Mn deoxidation [5], boron addition to modify inclusions [6], and low basicity top slag refining [7] and Na<sub>2</sub>CO<sub>3</sub> addition to modify inclusions [8].

On the other hand, there are still some problems that plagued metallurgical workers for many years, but which the subjects of new research and breakthroughs in recent years [9–13]. For example, in terms of the formation mechanism and evolution of SiO<sub>2</sub>-type inclusions in Si-Mn killed steel wires, Wang et al. [9,10] found, in 2015, that the formation mechanism of SiO<sub>2</sub>-type inclusions in wire rods involves two main steps: First, solid SiO<sub>2</sub> phase precipitates form MnO-SiO<sub>2</sub>-Al<sub>2</sub>O<sub>3</sub> system inclusions during the casting process to form dual-phase inclusions in the as-cast bloom, and second, dual-phase inclusions experience phase separation during the rolling process for heterogeneity and

great compression ratios [9,10]. However, some of their results are not very persuasive. For example, they only analysed the inclusions in tundish and cast-bloom, but not in wire rod. As we know, dual-phase inclusions may experience phase separation during the drawing process for heterogeneity and great compression ratio. Thus, the formation mechanism and evolution of SiO<sub>2</sub>-type inclusions in Si-Mn killed steel wires should be studied further. With regard to the formation mechanism of CaO-SiO<sub>2</sub>-Al<sub>2</sub>O<sub>3</sub>-(MgO) inclusions, there were some controversies until Wang et al. [11,12] did some research in 2017 and came up with a very persuasive view. Wang et al. pointed out that it can be reasonably concluded that CaO-SiO<sub>2</sub>-type inclusions in saw wire were exogenous particles from entrapped/emulsified top slag, but not products of slag-steel-inclusion chemical reactions [11,12]. However, this argument has not been confirmed by others or recognized by fellow researchers.

For the factors influencing oxide inclusion, deformability under high and low temperatures had not been noticed until Zhang et al. [13] did some research in 2018. They came up with a theory that the deformability of oxide inclusion under different temperatures could be scaled by Young's moduli. However, some of the results are not very persuasive. For example, the theory of the influence of temperature on the deformability of oxide inclusions has not been confirmed by experiments.

Few researchers have looked at changing the chemical composition of LF refining (ladle furnace) slag with new components to improve inclusions absorption. The influence of alkali oxides enhancing inclusion removal had not been noticed until Sohn et al. [14,15] did some research at 2014. The effect of alkali oxides (Li<sub>2</sub>O, Na<sub>2</sub>O, K<sub>2</sub>O, Rb<sub>2</sub>O, Cs<sub>2</sub>O) containing tundish fluxes on inclusion removal have been studied; the results indicated that K<sub>2</sub>O, Rb<sub>2</sub>O, and Cs<sub>2</sub>O addition seems to significantly enhance inclusions removal, but the influence of Li<sub>2</sub>O and Na<sub>2</sub>O has the opposite effect. In detail, not only the number of inclusions, but also the average inclusions diameter, increased with minimal improvement with Li<sub>2</sub>O and Na<sub>2</sub>O addition. Sohn et. al came up with an explanation that K<sup>+</sup>, Rb<sup>+</sup> and Cs<sup>+</sup> have a large cationic radius compared to Li<sup>+</sup> and Na<sup>+</sup>; therefore, the inclusions can be sufficiently entrained within the slag once absorbed due to the significant increase in the viscosity. However, they did not give any more detailed explanation about how the increase in viscosity of slag can improve the absorption ability of inclusions.

On the other hand, the alkali oxides have not been applied in LF refining progress until now. The influence of alkali oxides on the number, size, morphology, and composition (especially for MnO-SiO<sub>2</sub>-Al<sub>2</sub>O<sub>3</sub> and CaO-SiO<sub>2</sub>-Al<sub>2</sub>O<sub>3</sub> inclusion systems) is still not completely understood.

Therefore, we have explored the influence of alkali oxides on enhancing inclusion removal by adding 2.5 wt%, 5.0 wt%, and 7.5 wt% Na<sub>2</sub>O and Rb<sub>2</sub>O into synthetic LF refining slag. The influence of alkali oxides (Na<sub>2</sub>O, Rb<sub>2</sub>O) on the number, average diameter, composition, and morphology of inclusions has been studied. Furthermore, we came up with a more detailed explanation about how the increase in viscosity of slag can improve the absorption ability of inclusions.

## 2. Experiment

### 2.1. Experimental Apparatus and Procedure

With respect to simulating LF refining progress, the MoSi<sub>2</sub> furnace was utilized to fabricate the C96V saw wire steels in this experiment. A schematic diagram of the experimental equipment is shown in Figure 1.

In this experiment, the temperature of liquid metal is continuously measured by means of a B-type reference thermocouple. An argon atmosphere was kept in experiments all the time, blowing from the bottom to the top of the furnace tube. The experimental procedures were carried as follows. Firstly, 1.00 kg industrial pure iron is placed into a MgO crucible of 60 × 10<sup>-3</sup> m (60 mm) inner diameter and 80 × 10<sup>-3</sup> m (80 mm) depth. Secondly, the crucible is placed in a graphite crucible to prevent liquid metal from leaking. Finally, after the whole crucible is placed in the chamber, the power is switched on and the furnace is heated to the experimental temperature [1873 K (1600 °C)].

Alloys were added into the melts when the temperature reached 1873 K (1600 °C). Sampling No. 0 is the original chemical composition in steel without interaction of slag and metal. After that, 0.05 kg synthetic LF refining slag was put onto the surface of the molten metal by corundum funnel (Shandong Hao Yang wear resistant material Co., Ltd., Zibo, China). The height of solid slag and liquid slag are about  $2.0 \times 10^{-2}$  m (2.0 cm) and  $1.5 \times 10^{-2}$  m (1.5 cm); it completely covered the surface of the metal. Samples No.1 to No. 3 are taken from the molten metal after the slag melted for 15, 30, and 45 min. After each sampling, the steel liquid is stirred with a graphite rod for 2 min to make the molten steel and the refining slag uniform. All of the samples are taken by quartz tube sampler and quenched immediately in water.

In total, there are 7 heats made by treating with different synthetic LF refining slags, to which were added 2.5 wt%, 5.0 wt%, and 7.5 wt% Na<sub>2</sub>O and Rb<sub>2</sub>O, as shown in Table 1. Samples were taken at 0, 15, 30, and 45 min during the refining progress.

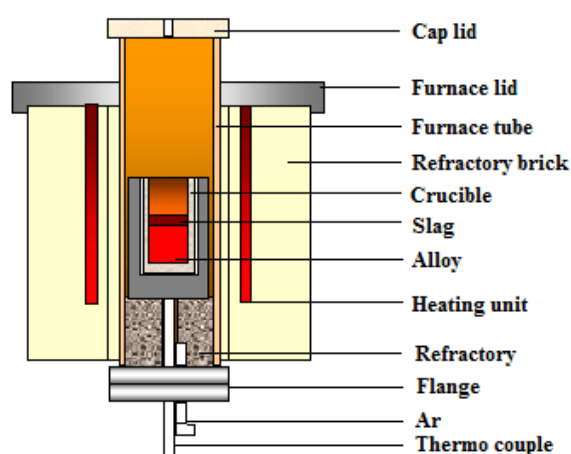


Figure 1. Schematic diagram of experimental equipment (MoSi<sub>2</sub> furnace).

Table 1. Chemical composition of synthesized refining slag.

Heat Number	CaO (wt%)	SiO <sub>2</sub> (wt%)	Al <sub>2</sub> O <sub>3</sub> (wt%)	Na <sub>2</sub> O (wt%)	Rb <sub>2</sub> O (wt%)	Time/min	CaO/SiO <sub>2</sub>
0 <sup>#</sup>	42.22	52.78	5.00	-	-	0, 15, 30, 45	0.8
1 <sup>#</sup>	40.11	50.14	4.75	2.50	-	0, 15, 30, 45	0.8
2 <sup>#</sup>	38.00	47.50	4.50	5.00	-	0, 15, 30, 45	0.8
3 <sup>#</sup>	35.89	44.86	4.25	7.50	-	0, 15, 30, 45	0.8
4 <sup>#</sup>	40.11	50.14	4.75	-	2.50	0, 15, 30, 45	0.8
5 <sup>#</sup>	38.00	47.50	4.50	-	5.00	0, 15, 30, 45	0.8
6 <sup>#</sup>	35.89	44.86	4.25	-	7.50	0, 15, 30, 45	0.8

## 2.2. Analysis Methods

A direct reading spectrometer was utilized to detect the composition of Si, Mn, P, Cr, V, Ni, and Cu. Steel samples were also sent to Analysis and Testing Center (Chemical Laboratory, Shenyang, China) of Northeastern University to analyse Al content by the ICP (Inductively Coupled Plasma) method. For C and S, an infrared C/S analyzer was applied. Then, the LECO<sup>®</sup> TC 500 O<sub>2</sub>/N<sub>2</sub> analyzer (LECO, San Jose, MI, USA) was chosen to detect O and N. The chemical composition of C96V saw wire steel is shown in Table 2.

**Table 2.** Chemical composition of C96V saw wire steels (mass %).

Heat Number	C	Si	Cr	Mn	V	[Al]s	T.O	N	P	S	Ni	Cu
0 <sup>#</sup>	0.96	0.16	0.21	0.34	0.10	≤0.0003	0.0012	0.0027	0.0067	0.0026	0.0027	0.0036
1 <sup>#</sup>	0.96	0.15	0.21	0.36	0.10	≤0.0003	0.0013	0.0033	0.0070	0.0032	0.0028	0.0041
2 <sup>#</sup>	0.97	0.15	0.20	0.35	0.11	≤0.0003	0.0012	0.0031	0.0071	0.0031	0.0031	0.0039
3 <sup>#</sup>	0.95	0.17	0.23	0.35	0.11	≤0.0003	0.0014	0.0033	0.0072	0.0034	0.0029	0.0041
4 <sup>#</sup>	0.96	0.15	0.20	0.34	0.12	≤0.0003	0.0015	0.0030	0.0070	0.0030	0.0022	0.0038
5 <sup>#</sup>	0.96	0.15	0.21	0.36	0.11	≤0.0003	0.0012	0.0028	0.0068	0.0029	0.0035	0.0036
6 <sup>#</sup>	0.97	0.16	0.20	0.37	0.10	≤0.0003	0.0013	0.0029	0.0061	0.0032	0.0033	0.0033

All of these steel samples were treated by 100–2000 mesh sand papers and polished. After that, photos (more than 50 pieces) around “S” route were taken. (On the surface of the sample, photos were taken in order from right to left, followed by from left to right). The Image J software (Image J 1.48, National Institutes of Health, Bethesda, MD, USA, 2014) was used for statistics of the size and count of inclusions; this software is a public domain, Java-based image processing program developed at the National Institutes of Health (NIH).

Finally, the metal samples were analysed by scanning electron microscope (SEM; Carl Zeiss AG, Niedersachsen, Germany) and Energy Dispersion Spectrum (EDS; Carl Zeiss AG, Niedersachsen, Germany) to determine the morphology and component of inclusions.

### 3. Results

#### 3.1. Effect of $\text{Na}_2\text{O}$ and $\text{Rb}_2\text{O}$ on the Variation in Inclusion Diameter

Figure 2 shows the effect of reaction time on the average non-metallic inclusion diameter with the addition of  $\text{Na}_2\text{O}$  or  $\text{Rb}_2\text{O}$ . For normal heat, it is obvious that the count descends slowly with refining time being raised from 15 to 45 min.

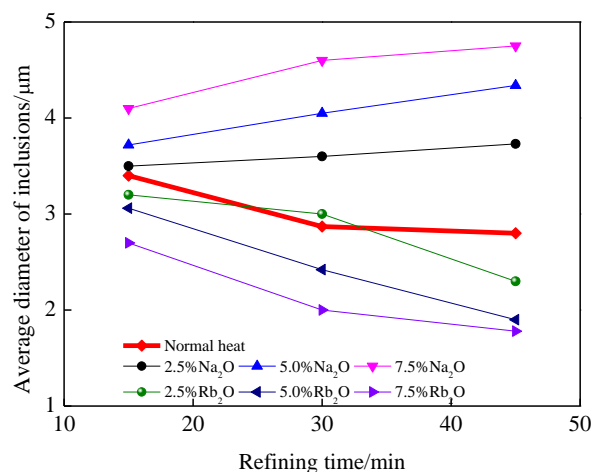


**Figure 2.** The average diameter of inclusion in experimental steel varies with refining time.

The addition of  $\text{Na}_2\text{O}$  in Figure 2 shows that the inclusion diameter with the addition of  $\text{Na}_2\text{O}$  gets larger than that at normal heat at all sampling times; what is worse, increments in  $\text{Na}_2\text{O}$  seem to increase the inclusion diameter observed in steel samples, suggesting that  $\text{Na}_2\text{O}$  is not at all a suitable candidate for enhancing inclusion removal in C96V saw wire steels.

Contrary to  $\text{Na}_2\text{O}$  addition,  $\text{Rb}_2\text{O}$  addition seems to yield a dramatic trend of decreased average inclusion diameter with increasing reaction time. (i) Under the same refining time, the average diameter of inclusions was reduced sharply with the content of  $\text{Rb}_2\text{O}$  raised from 2.5% to 7.5%; (ii) On the other

hand, the average diameter of inclusions decreased rapidly with the refining time ascending from 15 to 45 min when the weight percentage of  $\text{Rb}_2\text{O}$  fixed. (iii) Furthermore, the average diameter of inclusions in steel samples which were treated by  $\text{Rb}_2\text{O}$  (4<sup>#</sup>, 5<sup>#</sup>, 6<sup>#</sup>) was smaller than that of normal heat (0<sup>#</sup>).

### 3.2. Effect of $\text{Na}_2\text{O}$ and $\text{Rb}_2\text{O}$ on Inclusion Distribution Overlayed on the Phase Diagram

Figure 3 describes the distribution of inclusions in the  $\text{MnO-SiO}_2\text{-Al}_2\text{O}_3$  and  $\text{CaO-SiO}_2\text{-Al}_2\text{O}_3$  phase diagram in normal heat. It is obvious that the contents of  $\text{SiO}_2$  and  $\text{Al}_2\text{O}_3$  in inclusions increased gradually. In detail,  $\text{MnO-SiO}_2\text{-Al}_2\text{O}_3$  inclusion mainly concentrate in the area of 70–90 wt%  $\text{SiO}_2$ , <18 wt%  $\text{Al}_2\text{O}_3$ ,  $\text{CaO-SiO}_2\text{-Al}_2\text{O}_3$  inclusion mainly concentrate in the area of 40–60 wt%  $\text{SiO}_2$ , 10–25 wt%  $\text{Al}_2\text{O}_3$  after the steels are refined with 2700 s (45 min). In addition, some  $\text{CaO-SiO}_2\text{-Al}_2\text{O}_3$  inclusions have a small amount of mass fraction of  $\text{CaO}$  and  $\text{Al}_2\text{O}_3$  below 10 wt%.

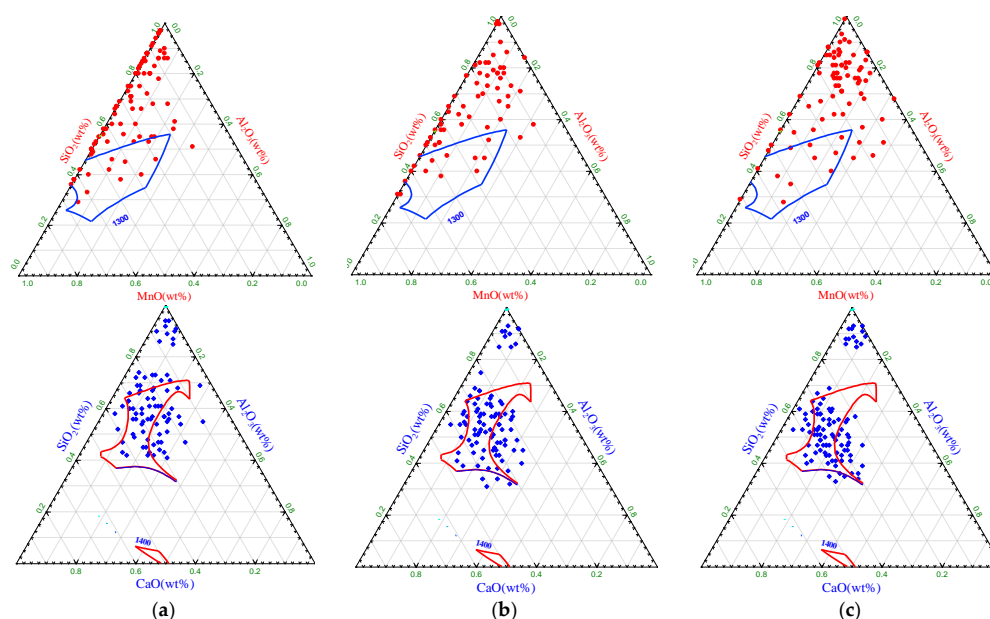


**Figure 3.** Inclusion distribution overlaid on phase diagram with refining time in 0<sup>#</sup> steel sample: (a) 900 s (15 min); (b) 1800 s (30 min); (c) 2700 s (45 min).

The inclusion distribution overlaid in phase diagram with different refining time in 2<sup>#</sup> (5.0 wt%  $\text{Na}_2\text{O}$ ) steel samples is shown in Figure 4. Obviously, with the 15 min reactions shown in Figure 4a, the distribution of inclusions seems to be dominant toward the  $\text{SiO}_2$ -rich region. With longer reaction times, the distribution of inclusions are spread across the ternary phase diagram with the addition of  $\text{Na}_2\text{O}$ .

Contrary to the effect of  $\text{Na}_2\text{O}$ , the  $\text{Rb}_2\text{O}$  on the average inclusion diameter generally has a decreasing trend with longer reaction times. Figure 5 describes the distribution of inclusions with  $\text{Rb}_2\text{O}$  content of 5.0 wt%. As the reaction time increased, there is a strong tendency for inclusions to be distributed toward the less  $\text{SiO}_2$  and  $\text{Al}_2\text{O}_3$  region. In detail, the  $\text{MnO-SiO}_2\text{-Al}_2\text{O}_3$  inclusion system mainly concentrate in the low melting area with 40–50 wt%  $\text{SiO}_2$ , <20 wt%  $\text{Al}_2\text{O}_3$ , and the  $\text{CaO-SiO}_2\text{-Al}_2\text{O}_3$  inclusion system mainly concentrate in the low melting area with 40–50 wt%  $\text{SiO}_2$ , <20 wt%  $\text{Al}_2\text{O}_3$  at the same time. For instance, the addition of  $\text{Rb}_2\text{O}$  seems to concentrate the distribution of inclusions toward the less  $\text{SiO}_2$ ,  $\text{Al}_2\text{O}_3$  phase, which is clearly shown in Figure 5.

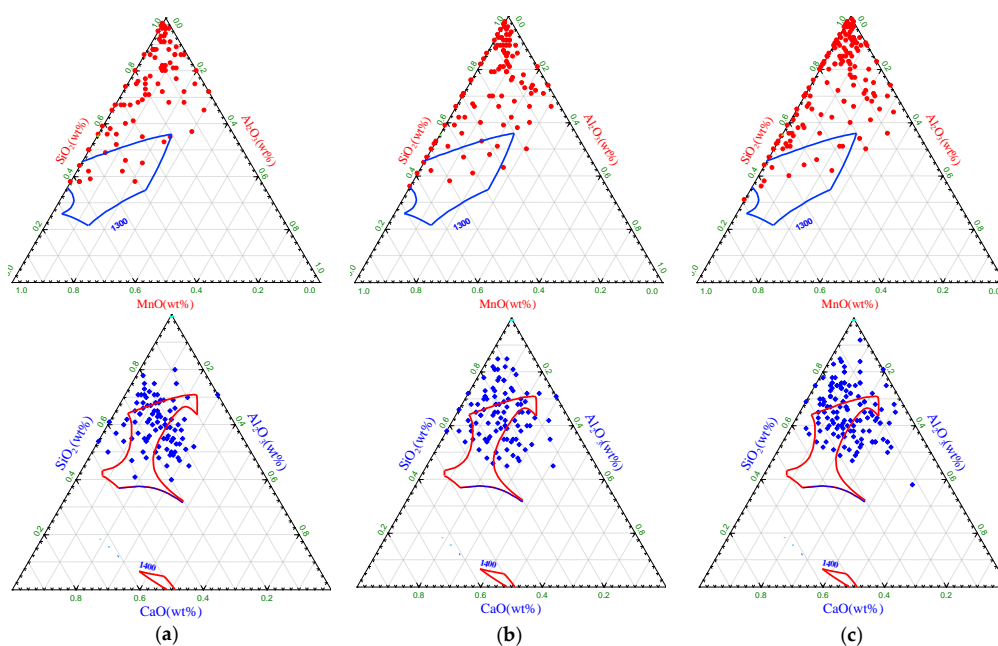


**Figure 4.** Inclusion distribution overlaid on phase diagram with refining time in 2<sup>#</sup> steel sample: (a) 900 s (15 min); (b) 1800 s (30 min); (c) 2700 s (45 min).

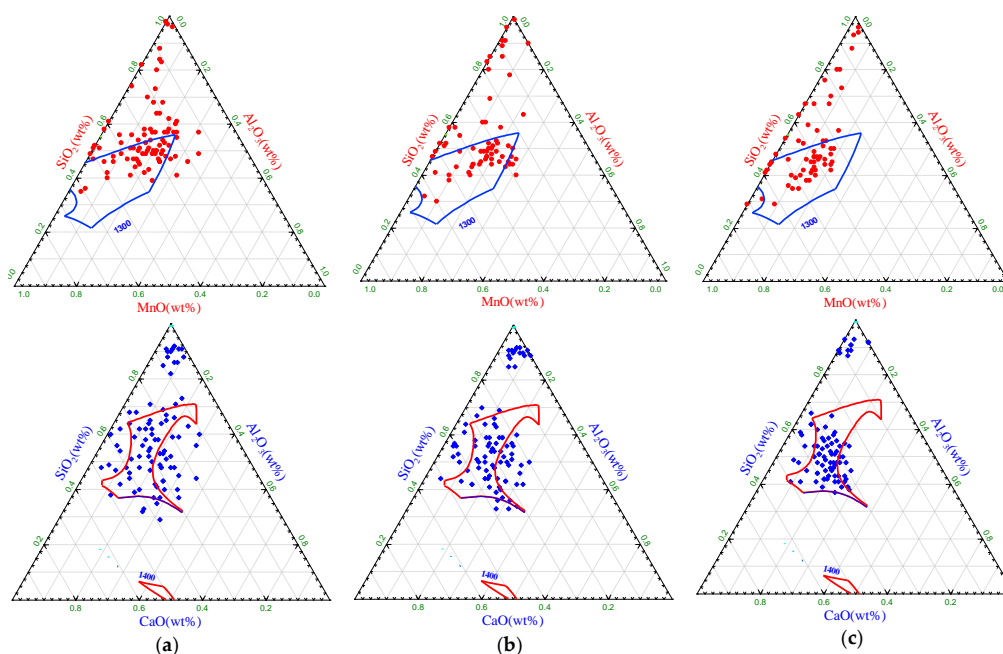


**Figure 5.** Inclusion distribution overlaid on phase diagram with refining time in 5<sup>#</sup> steel sample: (a) 900 s (15 min); (b) 1800 s (30 min); (c) 2700 s (45 min).

In summary, at longer reaction times, the distribution of inclusions is spread across the ternary phase diagram, and dominant more toward the  $\text{SiO}_2$  and  $\text{Al}_2\text{O}_3$  region, suggesting  $\text{Na}_2\text{O}$  addition and an increase in  $\text{Na}_2\text{O}$  would likely be detrimental to control inclusions systems concentrating in the low melting area. In contrast,  $\text{Rb}_2\text{O}$  addition would likely be helpful to control both  $\text{MnO}$ - $\text{SiO}_2$ - $\text{Al}_2\text{O}_3$  and  $\text{CaO}$ - $\text{SiO}_2$ - $\text{Al}_2\text{O}_3$  inclusion system concentrating in low melting area. This is also shown in Figure 6.

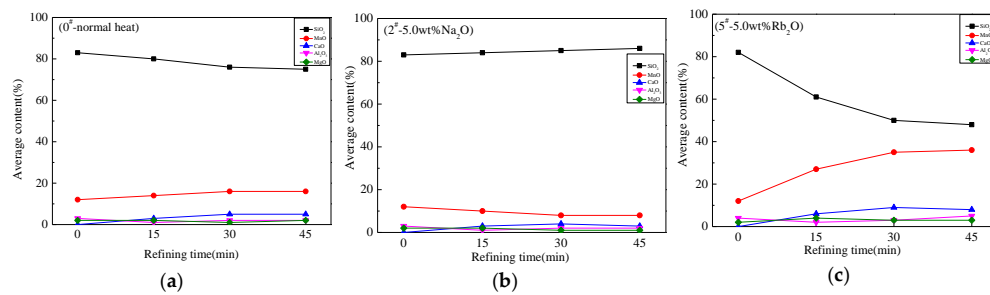
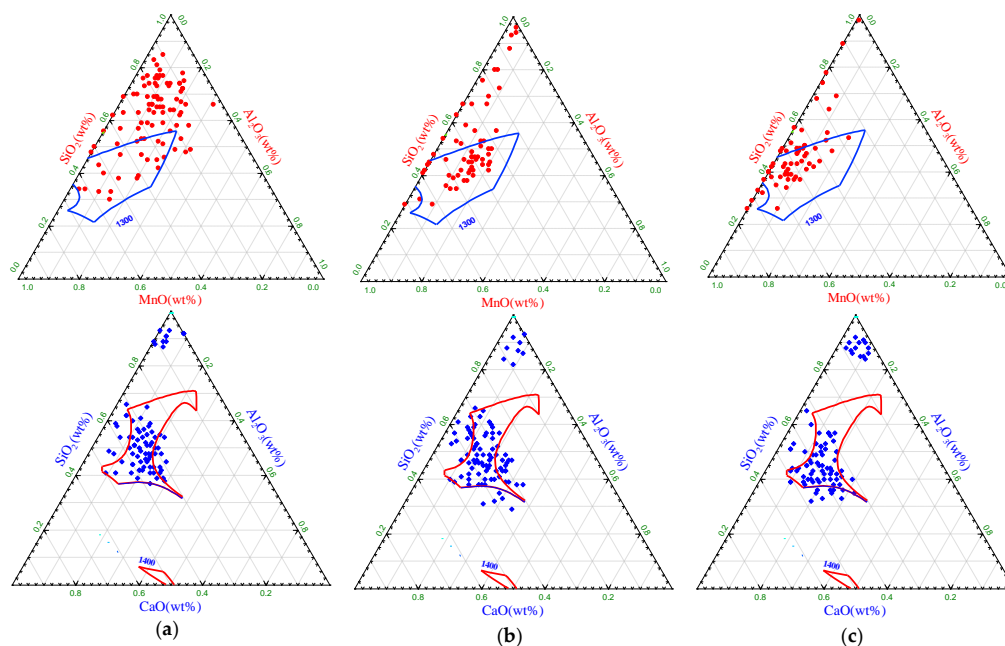


**Figure 6.** Average content of each component in inclusions during refining. (a) 0<sup>#</sup>, normal heat; (b) 2<sup>#</sup>, 5.0 wt% Na<sub>2</sub>O; (c) 5<sup>#</sup>, 5.0 wt% Rb<sub>2</sub>O.

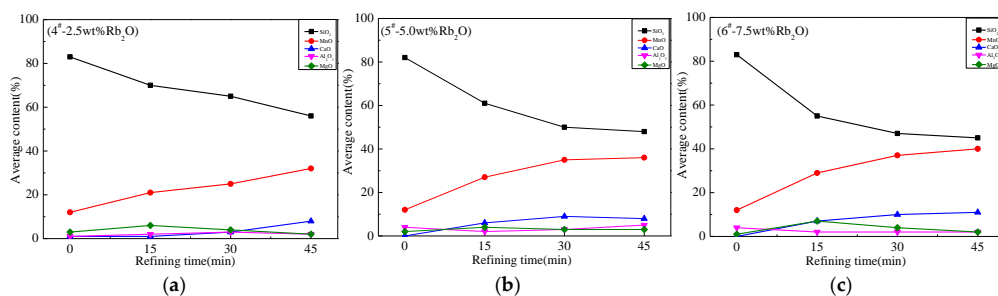
Figure 6 shows the average content of each component in inclusions during refining. Obviously, the content of SiO<sub>2</sub> and Al<sub>2</sub>O<sub>3</sub> in inclusions decreases sharply when the steel samples are treated by Rb<sub>2</sub>O, as shown in Figure 6c. Contrary to the effect of Rb<sub>2</sub>O, the effect Na<sub>2</sub>O on the content of SiO<sub>2</sub> and Al<sub>2</sub>O<sub>3</sub> in inclusions yielded generally an increasing trend with longer reaction times, as shown in Figure 6b.

Figure 7 compares the change in the inclusion chemistry within the MnO-SiO<sub>2</sub>-Al<sub>2</sub>O<sub>3</sub>, CaO-SiO<sub>2</sub>-Al<sub>2</sub>O<sub>3</sub> ternary phase diagrams after 2700 s (45 min) with varying amounts of Rb<sub>2</sub>O additions from 2.5 wt% to 7.5 wt%. Additionally, the average content of each component in inclusions during refining process is shown in Figure 8.

It may be noted that the MnO-SiO<sub>2</sub>-Al<sub>2</sub>O<sub>3</sub> and CaO-SiO<sub>2</sub>-Al<sub>2</sub>O<sub>3</sub> inclusions system were distributed toward the less SiO<sub>2</sub> and Al<sub>2</sub>O<sub>3</sub> phase with Rb<sub>2</sub>O addition increased from 0 wt% to 7.5 wt%.



**Figure 7.** Inclusion distribution overlaid on phase diagram as a function of refining 2700 s (45 min) with the synthetic refining slags containing 2.5–7.5 weight percentage Rb<sub>2</sub>O (a) 2.5 wt% Rb<sub>2</sub>O; (b) 5 wt% Rb<sub>2</sub>O; (c) 7.5 wt% Rb<sub>2</sub>O.



**Figure 8.** Average content of each component in inclusions during refining. (a) 4#, 2.5 wt% Rb<sub>2</sub>O; (b) 5#, 5 wt% Rb<sub>2</sub>O; (c) 6#, 7.5 wt% Rb<sub>2</sub>O.

### 3.3. Influence of Na<sub>2</sub>O and Rb<sub>2</sub>O on the Number of Inclusions

Figure 9 shows the influence of reaction time on the number of inclusions with the addition of Na<sub>2</sub>O or Rb<sub>2</sub>O. For normal heat, it can be noted that the number of inclusions reduced gently when the reaction time increased from 900 to 2700 s (15 to 45 min). For heats with Na<sub>2</sub>O additions from 2.5 wt% to 7.5 wt%, obviously, the number of inclusions exceeds normal level for all the concentrations of Na<sub>2</sub>O. However, unlike Na<sub>2</sub>O, reactions of the C96V saw wire steel samples with Rb<sub>2</sub>O containing synthesized refining slag samples resulted in a significant decrease in the number of inclusions observed with both longer reaction times and higher concentrations of Rb<sub>2</sub>O, as observed in Figure 9.

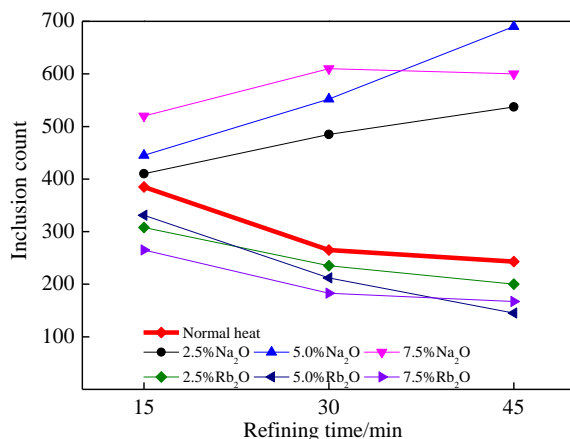


**Figure 9.** The count of inclusion in experimental steel varies with different refining time.

### 3.4. Morphology and Element Distribution of Typical Inclusions

Morphological observations of typical inclusions by SEM-EDS are shown in Figures 10–12. The majority of inclusions in all of the experimental heats are SiO<sub>2</sub>-MnO-Al<sub>2</sub>O<sub>3</sub> and SiO<sub>2</sub>-CaO-Al<sub>2</sub>O<sub>3</sub> systems, the differences about inclusion components, sizes and numbers have been discussed above.

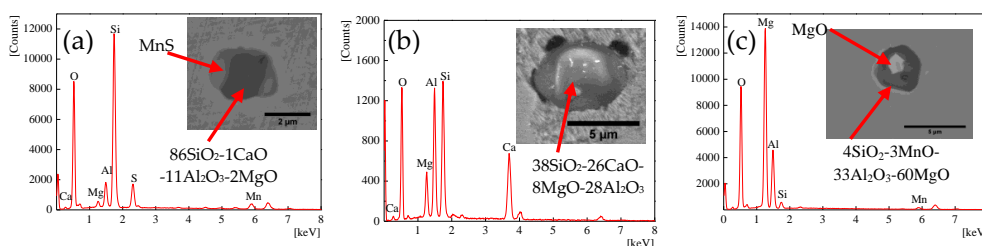


**Figure 10.** Typical inclusions at the normal experimental heat.

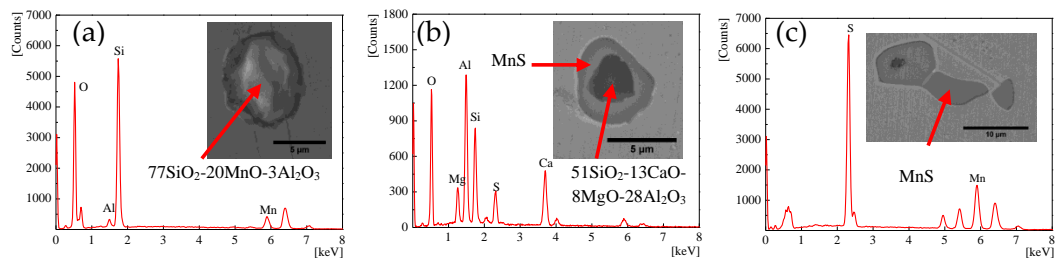


**Figure 11.** Typical inclusions in steel which were treated by adding  $\text{Na}_2\text{O}$  in synthetic refining slag.

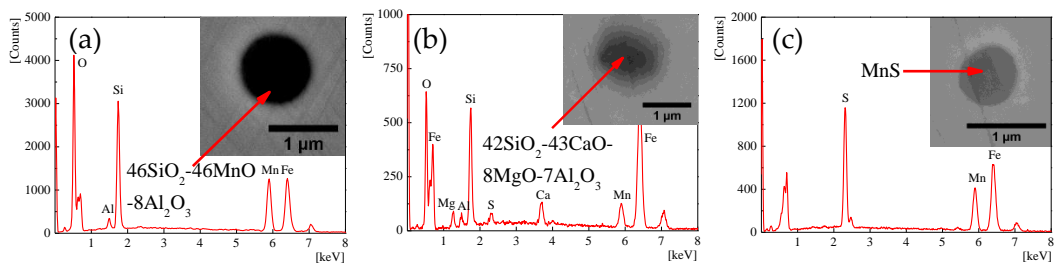


**Figure 12.** Typical inclusions in steel which were treated by adding  $\text{Rb}_2\text{O}$  in synthetic refining slag.

It is obvious that the size of inclusions in normal heat is around  $5\ \mu\text{m}$ , as shown in Figure 10. However, this increased sharply after the steel samples were treated by  $\text{Na}_2\text{O}$ ; some are large than  $20\ \mu\text{m}$ , as shown in Figure 11. In contrast, inclusions became very small, with diameters of about only  $1\ \mu\text{m}$  after steel samples were treated with  $\text{Rb}_2\text{O}$ , as shown in Figure 12.

### 3.5. Element Distribution in Complex Inclusion

As mentioned, complex inclusions were discovered in all of the experimental steel samples. In order to describe inclusion structures exactly, SEM mappings were done, as shown in Figures 13–15. Obviously, both  $\text{MnO-SiO}_2\text{-Al}_2\text{O}_3$  and  $\text{CaO-SiO}_2\text{-Al}_2\text{O}_3$  inclusions are multi-layered composite structures in all experimental steel samples. In detail, there was a  $\text{SiO}_2$ ,  $\text{MnO}$ ,  $\text{CaO}$ , and  $\text{Al}_2\text{O}_3$  homogeneous composite in the center, and a periphery of  $\text{MnS}$  precipitate around it.

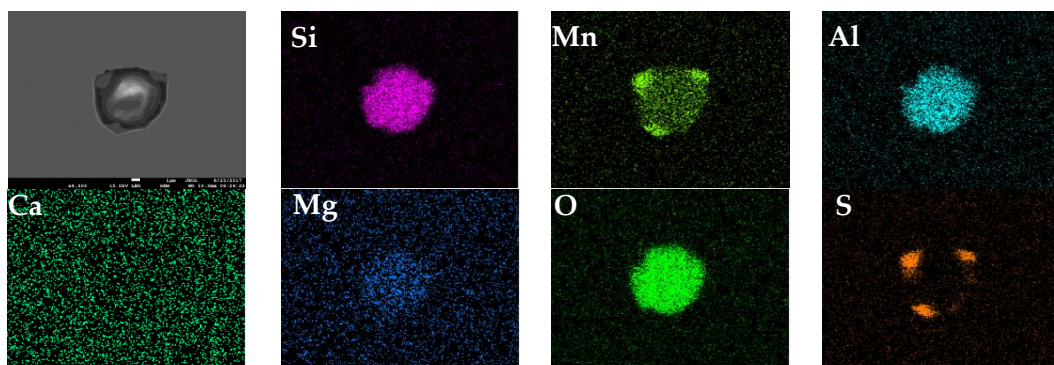


**Figure 13.** SEM mapping of typical inclusions in normal experiment heat.

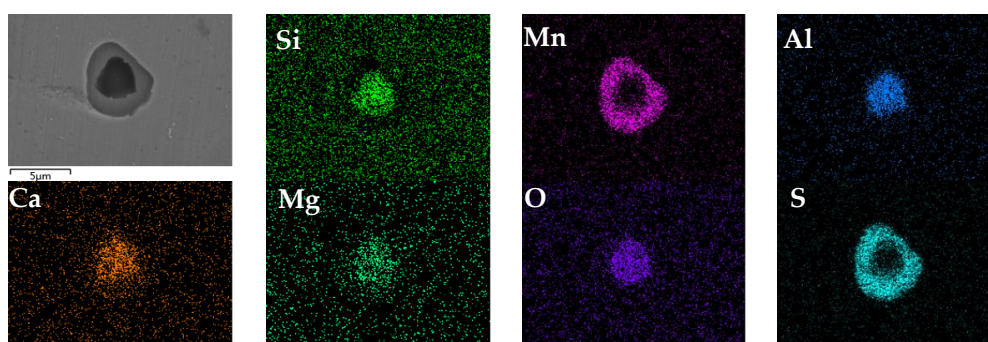


**Figure 14.** SEM mapping of typical inclusions in steel treated with synthetic refining slag containing  $\text{Na}_2\text{O}$ .

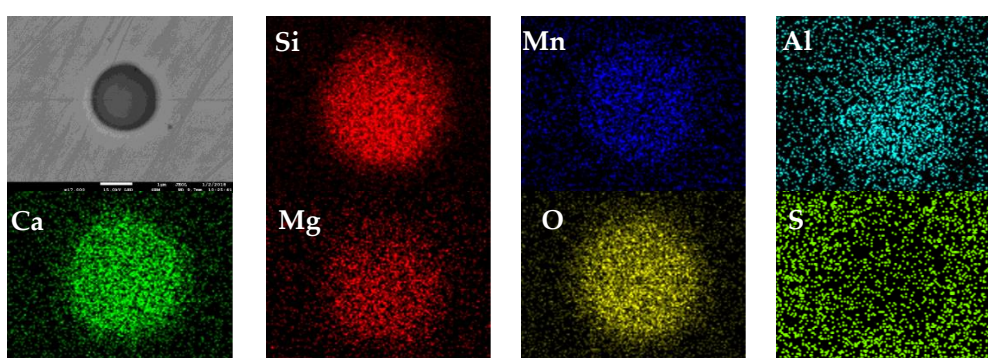


**Figure 15.** SEM mapping of typical inclusions in steel treated with synthetic refining slag containing  $\text{Rb}_2\text{O}$ .

#### 4. Discussion

The content of alkali oxides in metallurgical slag is usually low, but its influence is significant. This comprehensive change in the slag composition has a dramatic impact on the thermochemical and thermophysical properties of the slag, including its density, surface tension [16], and viscosity [17]. In particular, surface tension and viscosity have a direct impact on melt/slag separation efficiency, melt/slag reaction kinetics, and the permeability of the intermediate gases used for reduction and heat transfer.

##### 4.1. Influence of $\text{Na}_2\text{O}$ , $\text{Rb}_2\text{O}$ on the Structure and Viscosity of Metallurgical Slags

Studies that discuss the structure and properties of metallurgical slags have been reviewed by Waseda and Toguri [18,19]. It is well known that the increase of  $\text{Li}_2\text{O}$ ,  $\text{Na}_2\text{O}$  content in  $\text{SiO}_2\text{-CaO-Al}_2\text{O}_3\text{-R}_2\text{O}$  ( $\text{R} = \text{Li}, \text{Na}$ ) slag system could decrease the viscosity. Sukenaga et al. [20] studied the effect of  $\text{Na}_2\text{O}$  on the viscosity for  $\text{CaO-SiO}_2\text{-Al}_2\text{O}_3\text{-Na}_2\text{O}$  slag. The results indicated that the viscosity of this quaternary melts decreased sharply with increasing the additive content of  $\text{Na}_2\text{O}$ . Similar results are also noted in the literature [21,22]. However, the influence of  $\text{K}_2\text{O}$ ,  $\text{Rb}_2\text{O}$ , and  $\text{Cs}_2\text{O}$  is the opposite; this is due to the fact that the structure of  $\text{SiO}_2\text{-CaO-Al}_2\text{O}_3\text{-R}_2\text{O}$  ( $\text{R} = \text{Li}, \text{Na}, \text{K}, \text{Rb}, \text{Cs}$ ) slag would like to change owing to the effects of alkali oxides ( $\text{Li}_2\text{O}, \text{Na}_2\text{O}, \text{K}_2\text{O}, \text{Rb}_2\text{O}, \text{Cs}_2\text{O}$ ) [18–23].

Based on the laws studied by past researchers, we calculated the viscosities for the slag compositions in our experiment by Factsage 7.2 (Bale, C.W.; Pelton, A.D.; Thompson, W.T.; Eriksson, G.; Hack, K.; Chartand, P.; Deckerov, S.; Jung, I.H.; Melanson, J.; Petersen, S. Thermfact/CRCT (Montreal, QC, Canada), GTT-Technologies (Aachen, Germany), 2017) at 1873 K (1600 °C). In detail, the viscosities are 0.351 Pa·s (0<sup>#</sup>, normal heat), 0.343 Pa·s (1<sup>#</sup>, 2.5 wt%  $\text{Na}_2\text{O}$ ), 0.318 Pa·s (2<sup>#</sup>, 5.0 wt%  $\text{Na}_2\text{O}$ ), 0.273 Pa·s (3<sup>#</sup>, 7.5 wt%  $\text{Na}_2\text{O}$ ). The calculated results are in good agreement with the expected law.

According to the literature [24,25], the structure of slag is very complex, including chains, rings, and three-dimensional network structures, as shown in Figure 16.

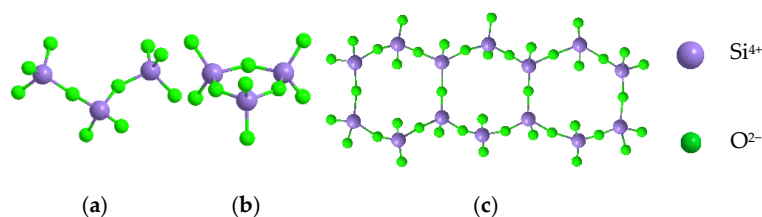
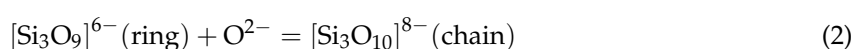


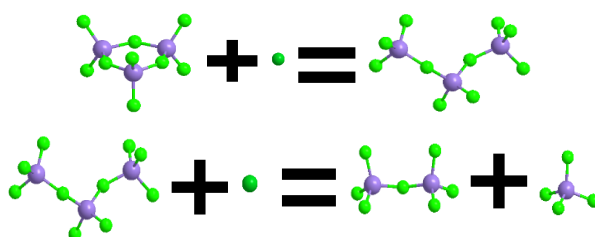
**Figure 16.** (a) Chains; (b) Rings; (c) Three-dimensional network structure.

(i) The influence of  $\text{Na}_2\text{O}$  on the viscosity of  $\text{SiO}_2\text{-CaO-Al}_2\text{O}_3$  slag can be understood when considering the change in the degree of polymerization (DOP) of slag structure [26].

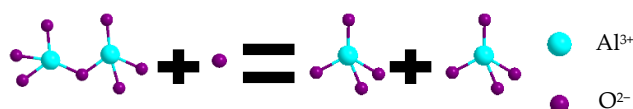


where  $\text{R}^+$  is the basic oxide cation such as  $\text{Na}^+$ . Addition of  $\text{Na}_2\text{O}$  would provide  $\text{O}^{2-}$ , which can modify the complex silicate structure into simple  $[\text{Si}_2\text{O}_7]^{6-}$  and  $[\text{SiO}_4]^{4-}$ . In addition, according to Sohn [14], after treatment with  $\text{Na}_2\text{O}$ , the  $[\text{AlO}_4]^{5-}$ -tetrahedral structure will be depolymerized. We have provided the schematic diagram for Equations (2) and (3) in Figure 17. A schematic diagram for how  $\text{Na}_2\text{O}$  can depolymerize the  $[\text{AlO}_4]^{5-}$ -tetrahedral structure is shown in Figure 18.

Therefore, the viscosity of slag decreases sharply.



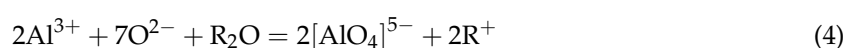
**Figure 17.** Schematic diagram of Equations (2) and (3).



**Figure 18.** Schematic diagram of  $\text{Na}_2\text{O}$  depolymerize the  $[\text{AlO}_4]^{5-}$ -tetrahedral structure.

(ii) The influence of  $\text{Rb}_2\text{O}$  and  $\text{Cs}_2\text{O}$  on the structure and properties of metallurgical slag have not been studied enough. Even so, some researchers [15,18,19] speculated that  $\text{Rb}_2\text{O}$  and  $\text{Cs}_2\text{O}$  have the same effect as  $\text{K}_2\text{O}$ . Furthermore, Sohn et al. [14,15] did some experiments to research the effect of  $\text{K}_2\text{O}$ ,  $\text{Rb}_2\text{O}$  and  $\text{Cs}_2\text{O}$  on inclusion removal based on the above inference. The results indicated that  $\text{Rb}_2\text{O}$ ,  $\text{Cs}_2\text{O}$  have the same effect as  $\text{K}_2\text{O}$ . In detail, with the introduction of the large cationic radius of the  $\text{K}^+$ ,  $\text{Rb}^+$  and  $\text{Cs}^+$  compared to  $\text{Na}^+$  and  $\text{Li}^+$ , the inclusions can be sufficiently entrained within the alumino-silicate-based slag once absorbed due to the significant increase in the viscosity.

It is well known that  $\text{K}_2\text{O}$  addition can catalyze the formation of  $[\text{AlO}_4]^{5-}$  tetrahedral units, which act as network formers in the slag structure [27–29], as expressed by Equation (4) [27]. A schematic diagram for Equation (4) is presented in Figure 19.



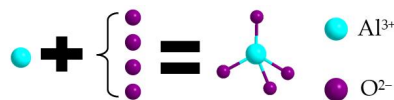


**Figure 19.** The schematic diagram of Equation (4).

Furthermore, according to Sohn et al. [14,15],  $K_2O$  addition could polymerize the slag to form complex aluminates and alumino-silicate structures. In order to help us understand this process, we provided the schematic diagram of how  $K_2O$ ,  $Rb_2O$  and  $Cs_2O$  polymerize the slag network structure (as shown in Figure 20). Thus, the viscosity of slag increases significantly with an increase in the content of  $Rb_2O$ .

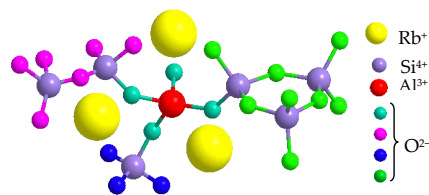


**Figure 20.** The schematic diagram of  $Rb_2O$  polymerize the slag network.

The schematic diagram of how  $Na_2O$  and  $Rb_2O$  change the structure of refining slag is shown in Figure 21. For the sake of understanding, we simplified the structure of refining, showing only the  $[AlO_4]^{5-}$ -tetrahedral structure, the Si-O-Al structure, and the Si-O- structure.

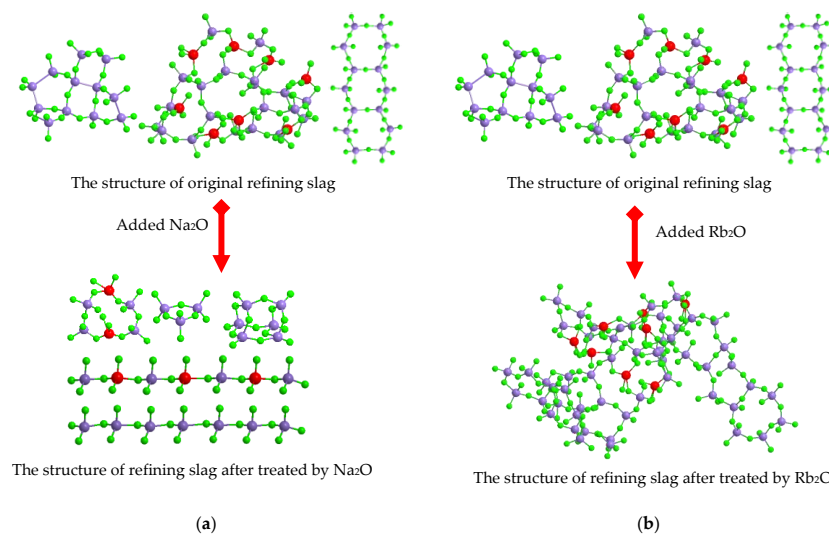


**Figure 21.** The structure of refining slag treated by alkali oxides (a)  $Na_2O$  addition, (b)  $Rb_2O$  addition.

#### 4.2. Influence of $Na_2O$ , $Rb_2O$ on the Ability of Slags to Absorb Inclusions

Most authors report that inclusion absorption by slag occurs in three stages [30–33]:

- (i) Flotation in the bath—transport of the inclusion to the steel/slag interface.
- (ii) Separation of liquid steel—movement of the inclusion to the interface, breaking the surface tension of steel.
- (iii) Dissolution in slag—removal of the inclusion from the steel/slag interface for full incorporation into the slag.

An inclusion can only be considered that is eliminated from steel when it is completely dissolved in the slag. According to Valdez et al. [31] and Reis et al. [34,35], the viscosity of slag significantly influences the ability of slag to absorb inclusions. Stage (i) takes place in molten steel; thus, the effect of Na<sub>2</sub>O and Rb<sub>2</sub>O occurs mostly in stages (ii) and (iii).

#### 4.2.1. The Slag Entrapment during Refining Process

The influence of alkali oxides (Li<sub>2</sub>O, Na<sub>2</sub>O, K<sub>2</sub>O, Rb<sub>2</sub>O, Cs<sub>2</sub>O) on the slag entrapment is an important factor that shouldn't be ignored. According to J. Strandh et al. [36], if the slag viscosity is too low, the risk of slag entrainment to the steel is promoted, resulting in more inclusions in the steel.

When Na<sub>2</sub>O was added to the slag, the reaction products ([Si<sub>3</sub>O<sub>9</sub>]<sup>6-</sup>, [Si<sub>3</sub>O<sub>10</sub>]<sup>8-</sup>, [Si<sub>2</sub>O<sub>7</sub>]<sup>6-</sup>, [SiO<sub>4</sub>]<sup>4-</sup>, [AlO<sub>4</sub>]<sup>5-</sup> and so on) from Equations (1)–(3) might be incorporated into the molten steel. Therefore, the number and average diameter of inclusion increased rapidly, and the content of SiO<sub>2</sub> and Al<sub>2</sub>O<sub>3</sub> contained in inclusions increased at the same time.

In contrast, the effect of Rb<sub>2</sub>O is the opposite. When Rb<sub>2</sub>O was added into slag, the slag entrapment during refining process was significantly weakened. Thus, the number and average diameter of inclusions, and the content of SiO<sub>2</sub> and Al<sub>2</sub>O<sub>3</sub> contained in inclusions, decrease sharply compared to normal heat; this is described in Figure 22.

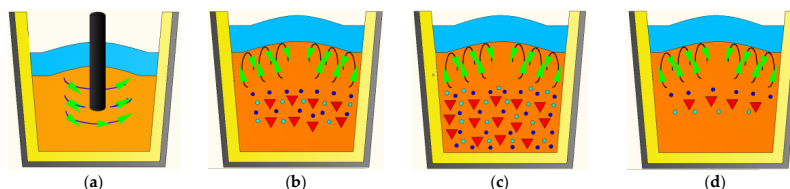


**Figure 22.** The schematic diagram of slag entrapment to the steel: (a) stirring steel by graphite rod; (b) normal heat; (c) added Na<sub>2</sub>O; (d) added Rb<sub>2</sub>O. The blue and orange part of the picture shows molten slag and molten steel respectively; Dots and triangles shows inclusions in steel; The arrows in (a) indicates the direction of the stirring of the graphite rod; The arrows in (b–d) indicates the flow direction of molten steel when slag entrapment happens during refining process.

#### 4.2.2. Influence of Na<sub>2</sub>O, Rb<sub>2</sub>O on the Second Stage: Separation of Liquid Steel

In terms of the second stage, Bouris et al. [37] and Nakajima et al. [38] have already done some correlative research, and described models for predicting the separation times for spherical, rigid, and chemically inert particles. During this process, the inclusion's motion is decided by a force balance between a capillary force ( $F_{\sigma,Z}$ ), a buoyancy force ( $F_b$ ), a drag force ( $F_d$ ) and a fluid force ( $F_m$ ), which is visualized in Figure 23. The force, when the inclusion is in contact with both steel and slag, are:

$$F_{\sigma,Z} = (-2\pi R_i + 2\pi Z)\sigma_{MS} + 2\pi R_i\sigma_{Si} - 2\pi R_i\sigma_{Mi} \quad (5)$$

$$F_b = \frac{4}{3}\pi R_i^3(\rho_s\tilde{\Delta}_b - \rho_i)g \quad (6)$$

$$F_d = 6\pi R_i\eta_s\tilde{B}_2 \frac{dZ}{dt} \quad (7)$$

$$F_m = \frac{1}{2}\frac{4}{3}\pi R_i^3\rho_s\tilde{\Delta}_b \frac{d^2Z}{dt^2} \quad (8)$$

$$\tilde{\Delta}_b = \frac{1}{4}\left(\frac{\rho_M}{\rho_s} - 1\right)\left(\frac{Z}{R_i}\right)^3 - \frac{4}{3}\left(\frac{\rho_M}{\rho_s} - 1\right)\left(\frac{Z}{R_i}\right)^2 + \frac{\rho_M}{\rho_s} \quad (9)$$

$$\tilde{B}_2 = 1 \text{ for } \frac{Z}{R_i} \geq 1$$

$$\left(\frac{\eta_M}{\eta_S} - 1\right) \left(\frac{Z}{R_i}\right)^2 - 2\left(\frac{\eta_M}{\eta_S} - 1\right) \left(\frac{Z}{R_i}\right) + \frac{\eta_M}{\eta_S}, \text{ for } 0 \leq \frac{Z}{R_i} \leq 1 \quad (10)$$

where  $R_i$  is the inclusion's radius,  $g$  is acceleration due to gravity,  $\rho_s$ ,  $\rho_i$  and  $\rho_M$  are the density of slag, inclusion and the metal, respectively.  $Z$ ,  $dZ/dt$  and  $d^2Z/dt^2$  is the inclusion's position, speed and acceleration,  $\eta_M$ ,  $\eta_s$  are the viscosity of metal and slag, respectively.  $\sigma_{MS}$ ,  $\sigma_{Si}$  and  $\sigma_{Mi}$  are the interfacial tensions between metal and slag, and slag and inclusion, and metal and inclusion, respectively.

The equation of motion is given by:

$$F_a + F_m = F_b - F_d - F_{\sigma,Z} \quad (11)$$

where  $F_a$  is the force from the acceleration of the inclusions, given as:

$$F_a = \frac{4}{3}\pi R_i \rho_i \frac{d^2Z}{dt^2} \quad (12)$$

Obviously, viscosity is an important factor on the stress of inclusions during the separation process, as shows in Equation (11). According to Valdez et al. [31], decreasing viscosity causes the inclusions easier enter into the slag. By contrast, that increasing viscosity causes the inclusions to require much more time to separate. Furthermore, in 2014, Yang [39] researched the influence of viscosity of slag on the separation time in depth, and observed the similar conclusions.

Therefore,  $F_a = F_b - F_d - F_{\sigma,Z} - F_m$  decreased gradually with the viscosity of slag increasing caused by  $Rb_2O$  addition. In other words,  $Rb_2O$  addition will exacerbate the kinetic conditions of inclusion removal during the separation stage due to  $Rb_2O$  addition decrease the viscosity of slag. By contrast, the effect of  $Na_2O$  addition is opposite. Namely,  $F_a = F_b - F_d - F_{\sigma,Z} - F_m$  increased gradually with the viscosity of slag decreasing caused by  $Rb_2O$  addition.

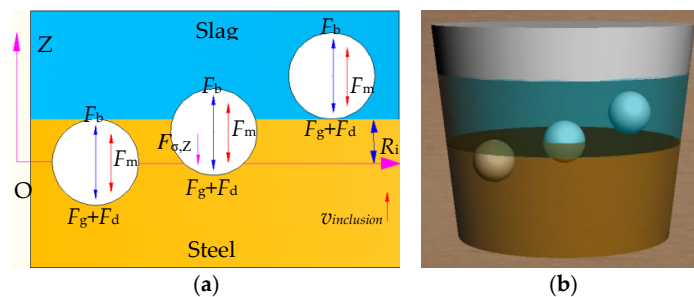


**Figure 23.** The schematic diagram of the force analysis of inclusions. (a) Force analysis of inclusions passing through steel slag interface; (b) Three dimensional simulation of inclusions passing through steel slag interface.

#### 4.2.3. Influence of $Na_2O$ , $Rb_2O$ on the Third Stage: Dissolution in Slag

Strandh et al. [36] developed a mathematical model to study inclusion behavior at the interface, and came up three types (remain, oscillating and pass) of inclusion behavior at the interface depending on the inclusion size, the velocity of the inclusion, and the interfacial properties of the system. Furthermore, Yang [39] put forward a supplement that a fourth type of inclusion behavior at the interface is “pass, and then return back”. We provided the schematic diagram of the four inclusion behaviors in Figure 24 in order to help the reader to understand these theories.

In  $Na_2O$  addition experiment heats, inclusions (especially for  $SiO_2$ -containing and  $Al_2O_3$ -containing inclusion) are difficult to dissolve into slag due to the depolymerization by  $Na_2O$ . In detail, inclusions (especially for  $SiO_2$ -containing and  $Al_2O_3$ -containing inclusion) will be depolymerized into smaller units with more simple structure, but not combine with slag units. As a result, inclusions may return back into molten steel, which is visualized in Figure 24d. Thus, the number and  $SiO_2$  and

$\text{Al}_2\text{O}_3$  content of inclusions increased remarkably with increasing not only reaction time, but also the content of  $\text{Na}_2\text{O}$ .

In contrast, in  $\text{Rb}_2\text{O}$  addition experiment heats, it is easy for inclusions (especially for  $\text{SiO}_2$ -containing and  $\text{Al}_2\text{O}_3$ -containing inclusion) to dissolve into slag due to the polymerization by  $\text{Rb}_2\text{O}$ . In detail, inclusions (especially for  $\text{SiO}_2$ -containing and  $\text{Al}_2\text{O}_3$ -containing inclusion) will be polymerized with slag units into larger units of more complex structure, and they will stay in the molten slag, which is visualized in Figure 24c. Thus, the number, average diameter, and  $\text{SiO}_2$  and  $\text{Al}_2\text{O}_3$  content of inclusions decreased significantly, not only with the reaction time but also the content of  $\text{Rb}_2\text{O}$ .

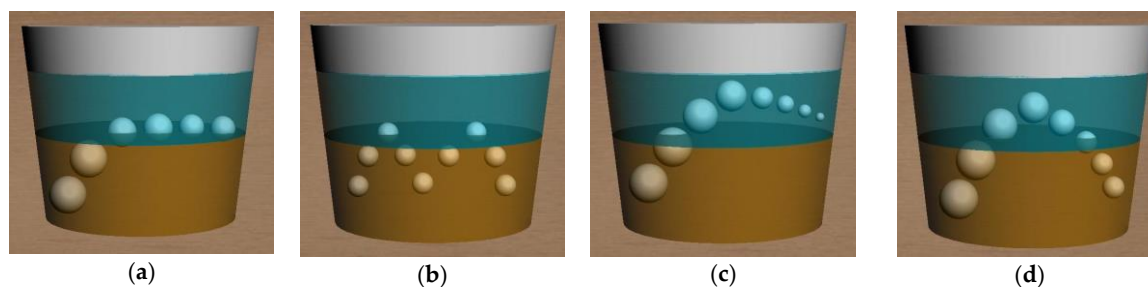


**Figure 24.** The four types of inclusion behavior at the steel-slag interface (a) Remain; (b) Oscillate; (c) Pass and dissolve; (d) Pass and then return back.

In summary, in order to understand the influence of  $\text{Na}_2\text{O}$  and  $\text{Rb}_2\text{O}$  on the ability of slag to absorb inclusions, its comprehensive effect on all of stages should be considered.

The schematic diagram of the dissolution model of inclusions in  $\text{Na}_2\text{O}$ -containing or  $\text{Rb}_2\text{O}$ -containing refining slag is shown in Figure 25. For the sake of understanding, we simplified the structure of refining and inclusions: only the  $[\text{AlO}_4]^{5-}$ -tetrahedral structure, the Si-O-Al structure and Si-O- structure are shown.

(i) For  $\text{Na}_2\text{O}$  addition experiment heats:

The inclusions (especially for  $\text{SiO}_2$ -containing and  $\text{Al}_2\text{O}_3$ -containing inclusion) may return back molten steel due to the fact that it is difficult to dissolve in slag, although it could dissolve through the molten-slag interface more easily. Additionally, the reaction products ( $[\text{Si}_3\text{O}_9]^{6-}$ ,  $[\text{Si}_3\text{O}_{10}]^{8-}$ ,  $[\text{Si}_2\text{O}_7]^{6-}$ ,  $[\text{SiO}_4]^{4-}$ ,  $[\text{AlO}_4]^{5-}$  and so on) from Equations (1)–(3) might be dissolved into molten steel, as shown in Figure 25a.

Therefore, the number and average diameter of inclusion increased rapidly, and the content of  $\text{SiO}_2$  and  $\text{Al}_2\text{O}_3$  contained in inclusions increased at the same time.

(ii) For  $\text{Rb}_2\text{O}$  addition experiment heats:

When the quantity of  $\text{Rb}_2\text{O}$  addition was low, most of the inclusions could pass through the molten-slag interface. It is easy for inclusions (especially for  $\text{SiO}_2$ -containing and  $\text{Al}_2\text{O}_3$ -containing inclusion) to be polymerized with slag units into larger units with more complex structure, and then remain in the molten slag. Additionally, slag entrapment during refining process will be significantly weakened. Therefore, the number and average diameter of inclusion decreased rapidly, and the content of  $\text{SiO}_2$  and  $\text{Al}_2\text{O}_3$  contained in inclusions decreased at the same time, as shown in Figure 25b.

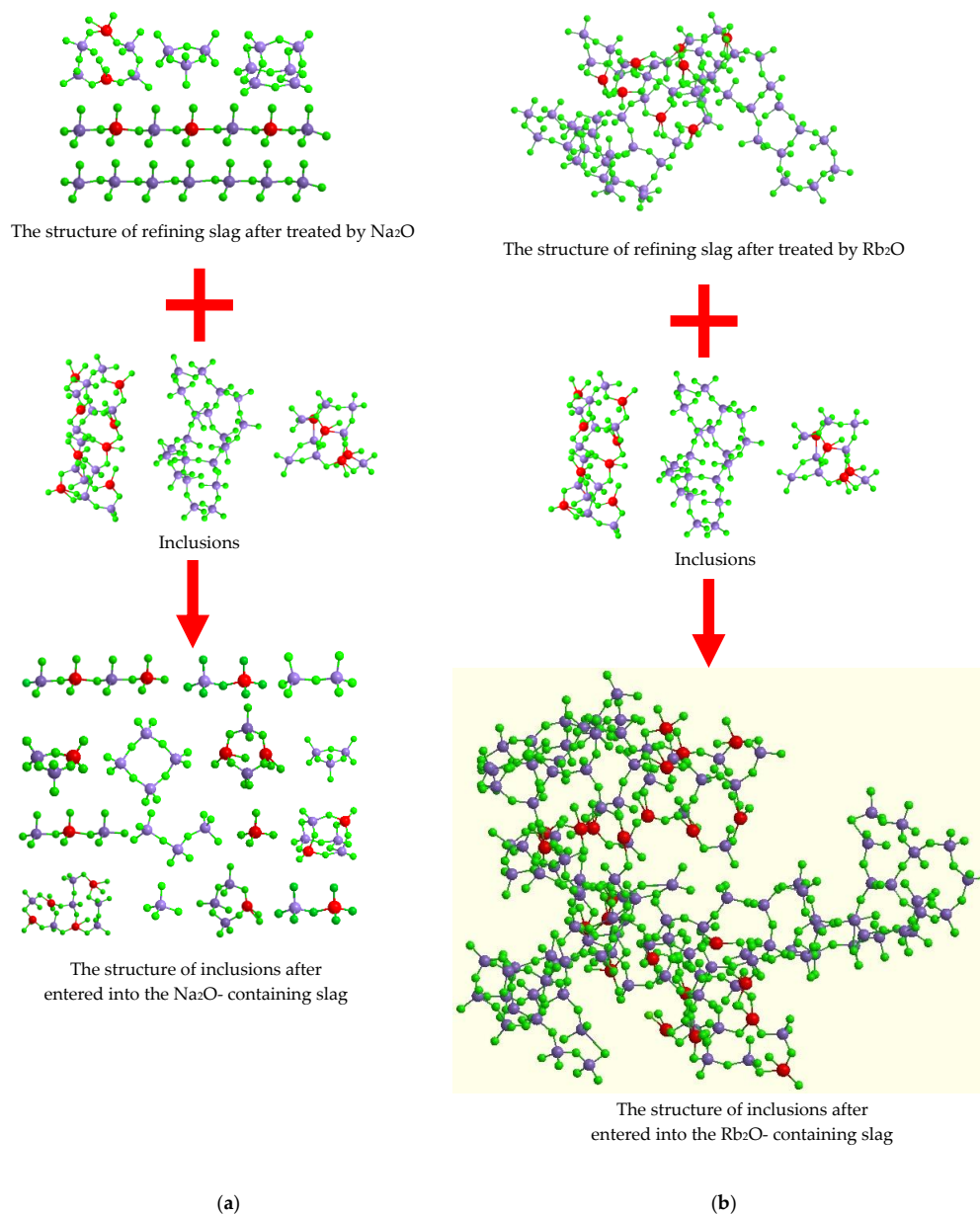


**Figure 25.** The schematic diagram of the dissolution model of inclusions in refining slag (a) containing  $\text{Na}_2\text{O}$ ; (b) containing  $\text{Rb}_2\text{O}$ .

## 5. Conclusions

The effect of  $\text{Na}_2\text{O}$  and  $\text{Rb}_2\text{O}$  containing synthetic LF refining slag on the absorption ability of inclusions for C96V saw wire steels has been studied. Kinetic studies using a  $\text{MoSi}_2$  furnace at 1873 K (1600 °C) on the reaction of synthetic LF refining slag containing alkali oxides ( $\text{Na}_2\text{O}$ ,  $\text{Rb}_2\text{O}$ ) with C96V saw wire steels suggested minimal improvement with  $\text{Na}_2\text{O}$  additions would deteriorate inclusion removal. In contrast,  $\text{Rb}_2\text{O}$  additions seems to remarkably enhance inclusion removal for to two reasons: after  $\text{Rb}_2\text{O}$  additions (i) the inclusions can be sufficiently absorbed into the refining slag due to the significant increase in the viscosity; (ii) the slag entrapment during refining process will be weakened dramatically. In detail, with  $\text{Rb}_2\text{O}$  additions:

(1) Not only did the number of inclusions, but also the average inclusion diameter, decrease in the steel samples;

(2) On the other hand, both of the MnO-SiO<sub>2</sub>-Al<sub>2</sub>O<sub>3</sub> and CaO-SiO<sub>2</sub>-Al<sub>2</sub>O<sub>3</sub> inclusion systems mainly concentrated in the low melting zone when the composition of Rb<sub>2</sub>O in synthetic refining slag was  $\geq 5.0$  wt%.

In summary, Rb<sub>2</sub>O additions seem to significantly improve the cleanliness in the as-quenched C96V saw wire steel melts, compared with preexisting synthetic refining slag compositions.

## 6. Future Work

It should be noted that much work needs to be done in future:

(i) the influence of stirring on slag entrainment that supported by rod. Obviously, there are many factors that should be considered in order to explore the influence of stirring on slag entrainment, such as the time of stirring, the velocity of stirring, the shape of the crucible, the diameter of the crucible, the diameter of the rod, the temperature of molten slag. (Other factors may also have important effects on the process, we can not describe all of them at present.)

(ii) The viscosities of CaO-SiO<sub>2</sub>-Al<sub>2</sub>O<sub>3</sub>-R<sub>2</sub>O (R = Na or Rb) should be measured. We got the viscosities of slag after Na<sub>2</sub>O addition by calculating with Factsage 7.2, but it must be measured in experiments, although the calculated results are in good agreement with the expected outcomes. Furthermore, we don't have any value about the viscosities of slag after Rb<sub>2</sub>O addition due to Factsage 7.2 lack of enough data base.

(iii) The influence of Na<sub>2</sub>O, Rb<sub>2</sub>O addition on the structure of slag (CaO-SiO<sub>2</sub>-Al<sub>2</sub>O<sub>3</sub>) should be researched further, especially for Rb<sub>2</sub>O addition. This is mainly because there is hardly any literature to have noticed this topic.

**Author Contributions:** C.C. and Y.L. conceived and designed the experiments; C.C., M.S. performed the experiments; C.C., M.S. and K.C. analyzed the data; Q.W. drew the schematic diagram in the article.; Z.J., Y.L. and H.L. contributed regants/materials/analysis tools; C.C. and M.S. wrote the paper.

**Acknowledgments:** The authors are grateful for the support from the National Key Research and Development Program of China (Grant No. 2016YFB0300105), and the Transformation Project of Major Scientific and Technological Achievements in Shenyang (Grant No. Z17-5-003), and the Fundamental Research Funds for the Central Universities (N172507002).

**Conflicts of Interest:** The authors declare no conflict of interest. The funding sponsors had no role in the design of the study; in the collection, analyses, or interpretation of data; in the writing of the manuscript; or in the decision to publish the results.

## References

1. Kirhara, K. Production technology of wire rod for high tensile strength steel cord. *Kobelco Technol. Rev.* **2011**, *30*, 62–65.
2. Zhang, L. Fluid flow, heat transfer and inclusion motion in a four-strand billet continuous casting tundish. *Steel Res. Int.* **2005**, *76*, 784–796. [[CrossRef](#)]
3. Fu, C.; Zhao, L. Fracture cause on SWRH72A hard wire. *Phys. Test* **2013**, *31*, 34–37.
4. Zhang, L. State of the art in the control of inclusions in tire cord steels—A review. *Steel Res. Int.* **2006**, *77*, 158–169. [[CrossRef](#)]
5. Chen, S.; Jiang, M.; He, X.; Wang, X. Top slag refining for inclusion composition transform control in tire cord steel. *Int. J. Min. Metall. Mater.* **2012**, *19*, 490–498. [[CrossRef](#)]
6. Cui, H.; Chen, W. Effect of boron on morphology of inclusions in tire cord steel. *J. Iron Steel Res. Int.* **2012**, *19*, 22–27. [[CrossRef](#)]
7. Maede, S.; Soejima, T.; Saito, T.; Matsumoto, T.; Fujimoto, H.; Mimura, T. Shape control of inclusions in wire rods for high tensile tire cord by refining with synthetic slag. In Proceedings of the 72th Steelmaking Conference, Chigago, IL, USA, 2–5 April 1989; pp. 379–385.
8. Chen, L.; Chen, W.; Hu, Y.; Chen, Z.; Xu, Y.; Yan, W. Effect of Na<sub>2</sub>CO<sub>3</sub> addition on inclusions in high-carbon steel for saw wire. *Trans. Indian Inst. Met.* **2018**, *71*, 383–391. [[CrossRef](#)]

9. Wang, K.; Jiang, M.; Wang, X.; Wang, Y.; Zhao, H.; Cao, Z. Formation mechanism of SiO<sub>2</sub>-type inclusions in Si-Mn-killed steel wires containing limited aluminum content. *Metall. Mater. Trans. B* **2015**, *46*, 2198–2207. [[CrossRef](#)]
10. Yang, W.; Guo, C.; Zhang, L.; Ling, H.; Li, C. Evolution of oxide inclusions in Si-Mn killed steels during hot-rolling process. *Metall. Mater. Trans. B* **2017**, *48*, 2717–2730. [[CrossRef](#)]
11. Wang, K.; Jiang, M.; Wang, X.; Wang, Y.; Zhao, H.; Cao, Z. Formation mechanism of CaO-SiO<sub>2</sub>-Al<sub>2</sub>O<sub>3</sub>-(MgO) inclusions in Si-Mn-killed steel with limited aluminum content during the low basicity slag refining. *Metall. Mater. Trans. B* **2016**, *47*, 282–290. [[CrossRef](#)]
12. Wang, K.; Jiang, M.; Wang, X.; Wang, Y.; Zhao, H.; Cao, Z. Study on formation mechanism of CaO-SiO<sub>2</sub>-Based inclusions in saw wire steel. *Metall. Mater. Trans. B* **2017**, *48*, 2961–2969. [[CrossRef](#)]
13. Zhang, L.; Guo, C.; Yang, W.; Ren, Y.; Ling, H. Deformability of oxide inclusions in tire cord steels. *Metall. Mater. Trans. B* **2018**, *49*, 803–811. [[CrossRef](#)]
14. Yu, J.; Kang, Y.; Sohn, I. Novel application of alkali oxides in basic tundish fluxes for enhancing inclusion removal in 321 stainless steels. *Metall. Mater. Trans. B* **2014**, *45*, 113–122. [[CrossRef](#)]
15. Choi, K.; Kang, Y.; Sohn, I. Effect of Rb<sub>2</sub>O and Cs<sub>2</sub>O on inclusion removal in 321 stainless steels using novel basic tundish fluxes. *Metall. Mater. Trans. B* **2016**, *47*, 1520–1526. [[CrossRef](#)]
16. Huang, X. *Principle of Iron and Steel Metallurgy*, 2nd ed.; Metallurgical Industry Press: Beijing, China, 2014; p. 328.
17. Mysen, B.; Richet, P. *Silicate Glasses and Melts: Properties and Structure*, 1st ed.; Elsevier: Amsterdam, The Netherlands, 2005.
18. Waseda, Y.; Toguri, J. *The Structure and Properties of Oxide Melts: Application of Basic Science to Metallurgical Processing*; World Scientific: Singapore, 1998; p. 113.
19. Waseda, Y.; Toguri, J. The structure of molten binary silicate systems CaO-SiO<sub>2</sub> and MgO-SiO<sub>2</sub>. *Metall. Mater. Trans. B* **1977**, *8*, 563–568. [[CrossRef](#)]
20. Sukenaga, S.; Saito, N.; Kawakami, K.; Nakashima, K. Viscosities of CaO-SiO<sub>2</sub>-Al<sub>2</sub>O<sub>3</sub>-(R<sub>2</sub>O or RO) melts. *ISIJ Int.* **2006**, *46*, 352–358. [[CrossRef](#)]
21. Kim, H.; Kim, W.H.; Park, J.H.; Min, D.J. A study on the effect of Na<sub>2</sub>O on the viscosity for ironmaking slags. *Steel Res. Int.* **2010**, *81*, 17–24. [[CrossRef](#)]
22. Zhen, Y.L.; Zhang, G.H.; Tang, X.L.; Chou, K.C. Influences of Al<sub>2</sub>O<sub>3</sub>/CaO and Na<sub>2</sub>O/CaO ratios on viscosities of CaO-Al<sub>2</sub>O<sub>3</sub>-SiO<sub>2</sub>-Na<sub>2</sub>O melts. *Metall. Mater. Trans. B* **2014**, *45*, 123–130. [[CrossRef](#)]
23. Sukenaga, S.; Haruki, S.; Nomoto, Y.; Saito, N.; Nakashima, K. Density and surface tension of CaO-SiO<sub>2</sub>-Al<sub>2</sub>O<sub>3</sub>-R<sub>2</sub>O (R = Li, Na, K) melts. *ISIJ Int.* **2011**, *51*, 1285–1289. [[CrossRef](#)]
24. Warren, B.; Krutter, H.; Morningstar, O. Fourier analysis of X-Ray patterns of vitreous SiO<sub>2</sub> and B<sub>2</sub>O<sub>3</sub>. *J. Am. Ceram. Soc.* **1936**, *19*, 202–206. [[CrossRef](#)]
25. Waseda, Y. Current structural information of molten slags by means of a high temperature X-ray diffraction. *Can. Metall. Q.* **1981**, *20*, 57–67. [[CrossRef](#)]
26. Maeda, M. *Advanced Physical Chemistry for Process Metallurgy*; Sano, N., Lu, W.K., Riboud, P.V., Eds.; Academic Press: San Diego, CA, USA, 1997; Volume 1.
27. Mysen, B.; Virgo, D.; Scarfe, C.; Cronin, D. Viscosity and structure of iron-and aluminum-bearing calcium silicate melts at 1 atm. *Am. Miner.* **1985**, *70*, 487–498.
28. Iguchi, Y.; Yonezawa, K.; Funaoka, Y.; Ban-ya, S.; Nishina, Y. Raman spectroscopic study on structure of binary silicates and ternary oxide melts with and without fluoride. In Proceedings of the 3rd International Conference on Molten Slags and Fluxes, Institute of Melts, University of Strathclyde, Glasgow, UK, 27–29 June 1988; p. 169.
29. Hwa, L.; Hwang, S.; Liu, L. Infrared and raman spectra of calcium aluminosilicate glasses. *J. Noncryst. Solids* **1998**, *238*, 193–197. [[CrossRef](#)]
30. Park, J.; Jung, I.; Lee, H. Dissolution behavior of Al<sub>2</sub>O<sub>3</sub> and MgO inclusions in the CaO-Al<sub>2</sub>O<sub>3</sub>-SiO<sub>2</sub> slags: Formation of ring-like structure of MgAl<sub>2</sub>O<sub>4</sub> and Ca<sub>2</sub>SiO<sub>4</sub> around MgO inclusions. *ISIJ Int.* **2006**, *46*, 1626–1634. [[CrossRef](#)]
31. Valdez, M.; Shannon, G.; Sridhar, S. The ability of slags to absorb solid oxide inclusions. *ISIJ Int.* **2006**, *46*, 450–457. [[CrossRef](#)]
32. Yi, K.; Tse, C.; Park, J.; Valdez, M.; Cramb, A.; Sridhar, S. Determination of dissolution time of Al<sub>2</sub>O<sub>3</sub> and MgO inclusions in synthetic Al<sub>2</sub>O<sub>3</sub>-CaO-MgO slags. *Scand. J. Metal.* **2003**, *32*, 177–184. [[CrossRef](#)]
33. ATLAS, AFS Inclusion. Inclusion Formation and Removal. Available online: <https://www.slideshare.net/msahisri/inclusion-formation-afs> (accessed on 12 February 2013).

34. Reis, B.; Bielefeldt, W.; Vilela, A. Absorption of non-metallic inclusions by steelmaking slags—A review. *J. Mater. Res. Technol.* **2014**, *3*, 179–185. [[CrossRef](#)]
35. Reis, B.; Bielefeldt, W.; Vilela, A. Efficiency of inclusion absorption by slags during secondary refining of steel. *ISIJ Int.* **2014**, *54*, 1584–1591. [[CrossRef](#)]
36. Strandh, J.; Nakajima, K.; Eriksson, R.; Jönsson, P. A mathematical model to study liquid inclusion behavior at the steel-slag interface. *ISIJ Int.* **2005**, *45*, 1838–1847. [[CrossRef](#)]
37. Bouris, D.; Bergeles, G. Investigation of inclusion re-entrainment from the steel-slag interface. *Metall. Mater. Trans. B* **1998**, *29*, 641–649. [[CrossRef](#)]
38. Nakajima, K.; Okamura, K. Inclusion. In Proceedings of the 4th International Conference on Molten Slags and Fluxes, Sendai, Japan, 8–11 June 1992; p. 505.
39. Yang, H.B. Study on Moving Behavior of Inclusions during Process of Passing Steel-Slag Interface. Ph.D. Thesis, University of Science and Technology Beijing, Beijing, China, 27 December 2014.



© 2018 by the authors. Licensee MDPI, Basel, Switzerland. This article is an open access article distributed under the terms and conditions of the Creative Commons Attribution (CC BY) license (<http://creativecommons.org/licenses/by/4.0/>).